International Journal of Engineering Research & Technology (IJERT)
ISSN: 2278-0181
Vol. 10 Issue 06, June-2021

To Evaluate the Burn-Perimeter of Star-Shaped Propellant Grain of A Solid Rocket Motor using Dimensionless Equations

[1]Aravind Rajan Ayagara, [2]Navya Shree Veerapaneni, [3]D. Govardhan
[1]Associate professor, [2]U.G Student, [3]Head of the department
Aeronautical Engineering, Institute of Aeronautical Engineering, Hyderabad, Telangana, India-500055

***Abstract*:- The main idea of my work is to discuss and evaluate the geometrical parameter like burn perimeter of the star-shaped propellant grain in detail. Whenever, solid propellant comes into the discussion, the grain design is one of the most important topics to be studied and evaluated. Because the thrust output as per requirement can be obtained by varying the shape of grain. Many scholars did lot of research on different sizes and shapes of grains that can provide the burn rate as per wanted. The star-shaped propellant grain design parameter like burn perimeter by using non-dimensional equations is evaluated. A MATLAB code is written in order to plot the non-dimensional burn-perimeter (*S/l*) versus burnt distance (*y* + *f*)/*l* for star-shaped propellant grain having star point, *n* = 6 for *θ* = 65°-75°. The obtained graphs for star points with different opening of star point angle in MATLAB are compared with burn perimeter values measured in CATIA V5 designing tool for corresponding set of values. Later, by taking the geometrical inputs like inner radius(*l*), fillet radius(*f*), web thickness(*w*) for star-shaped grain having star point, *n* = 6, the grain area regressive is modelled by using CATIA V5 design tool.**

Keywords:- Solid Rocket Motor Propellant Grain Burn perimeter Star-shape grain design

1. INTRODUCTION

The act of supplying a propelled force to a body that is initially at rest, causing it to change its velocity by overcoming the retarding forces present in the medium of that body is called *Propulsion.*

Jet propulsion is divided into two categories: rocket propulsion and duct propulsion. The distinction between rocket and duct propulsion is that rocket propulsion generates thrust by ejecting stored matter (propeller). Non-air-breathing engines are another name for rocket propulsion engines. Air-breathing engines are generally referred to as duct propulsion engines. The majority of the working fluid in a duct propulsion engine is its surroundings, along with some stored fuel.

Chemical combustion is the primary source of energy for rocket propulsion. Solar radiation and nuclear reactions are two other sources of energy that can be used to propel rocket engines.

The propellants are the materials that make up the chemical reactions that take place within a rocket motor.

Depending on whether the propellant is solid or liquid, chemical rocket motors are divided into two groups.

The propellant in a solid-propellant rocket is entirely contained inside the combustion chamber as one or more formed blocks known as grains, which are supported by the walls or special grids, traps, or retainer pads. A solid-propellant rocket's key feature is its simplicity; it doesn't even need a feed system. However, the burning time is limited to a few seconds or fractions of a second and seldom exceeds one or two minutes, though low-performance motors have achieved durations as long as ten or twenty minutes.

In the case of a liquid propellant, the propellant is said to be hypergolic if the two liquids provided ignite spontaneously as a result of simple mixing. Whenever the two constituents responsible for the reaction are contained in a single liquid (as in catalytic decompositions), this liquid is alluded to as a monopropellant.

As the applications of rocket motors depend on their special characteristics, knowing those characteristics in order to develop one is important. The main characteristics are indicated below:

a. The essential characteristic of rocket motors, the one which distinguishes them intrinsically from other types of jet power-plants, is that they do not make use of the surrounding air.
b. The rocket motor contains no moving parts (except perhaps certain auxiliaries in the feed system); its geometry is fixed and its operations is independent of the speed of flight, in contrast to the other jet systems in which the speed is limited by internal aerodynamic considerations. Only rockets are capable of operating at extremely high Mach numbers.
c. The high pressure in the combustion chamber (10 to 500 kg/cm^2) makes it possible to develop enormous quantities of energy for small volumes. For the same weight and size of powerplant, the rocket motor offers the highest thrust that can be obtained.
d. The necessity of carrying both the fuel and the oxidizer means that a rocket motor has a high specific consumption. The consumption is between 3 and 6 per ton (metric) of the thrust and per second, as compared with a fuel consumption of 0.25 to 0.3kg per ton and per second in the case of a turbojet at sea level.

1.1 *Basic Solid Rocket Motor*

A solid propellant rocket is formed by four main components as shown in fig 1.1.

International Journal of Engineering Research & Technology (IJERT)
ISSN: 2278-0181
Vol. 10 Issue 06, June-2021

- A case containing the solid propellant and withstanding internal pressure when the rocket is functioning.
- The solid propellant charge (or grain), which is typically bonded to the inner wall of the case, and occupies before ignition the greater a part of its volume. When burning, the solid propellant is transformed into hot combustion products. The volume occupied by the combustion products is called a combustion chamber.
- The nozzle channels the discharge of the combustion products and because of its shape accelerates them to supersonic velocity.
- The igniter, which can be a pyrotechnic device or a small rocket, starts the rocket operating when an electrical signal is received

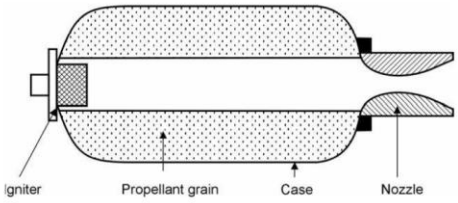

Figure 1.1: Basic solid rocket motor

1.2 *Thrust law*

It is possible with suitable grain designs, to obtain a thrust which increases (progressive burning), remains constant (neutral), decreases (regressive) or follows a wide variety of laws along the burning time.

With constant-geometry nozzles, the thrust is always approximately proportional to the chamber pressure (the thrust coefficient does not vary significantly). To show that the previous sentence is correct, a test was recorded of the thrust and pressure versus time. Fig 1.2 represents such a typical recording corresponding to a near-constant thrust, together with some current definitions of durations and thrust (or pressure) values. The integral of the thrust gives the impulse ***I***.

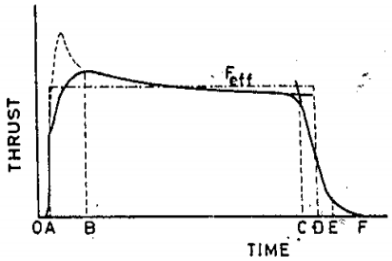

Figure 1.2: Thrust law.

1.3 *Propellant burning rate*

The combustion by parallel layers of a solid propellant is a progressive phenomenon entirely localized on the surface of the grain and the *burning rate* ***r*** is defined as the distance travelled per second by the flame front perpendicularly to the free surface of the grain (the ignition is assumed to be homogeneous).

Therefore, the combustion surface must vary in a foreseeable manner during the burning time and fissures or cracks in the grain must be strictly avoided because they may unexpectedly increase the surface and even induce local pressure build-ups and the associated stresses that tend to spread the fissure.

1.4 *Erosive burning*

The burning rate *r* of the solid propellant or propellant increases simultaneously with the increase in gas velocity of crossflow. The increased velocity which is dependent contribution to the burning rate *r* is said to be *Erosive Burning.*

2. LITERATURE REVIEW

When solid propellant comes into the discussion, the grain design is one of the most important topics to be studied and evaluated. Because the thrust output as per requirement can be obtained by varying the shape of grain.

Many scholars did lot of research on different sizes and shapes of grains that can provide the burn rate as per wanted.

Inside the rocket motor, the grain is a developed mass of processed solid propellant. The motor performance characteristics are determined by the propellant product and grain geometrical configuration. The propellant grain has a cast, moulded, or extruded body that reflects hard rubber or plastic in appearance and feel. It will burn on all of its exposed surfaces once ignited, producing hot gases that are then expelled through a nozzle. Just a few rocket motors have multiple grains in a single case or chamber, and even fewer grains have segments of separate propellant compositions. Most rockets, on the other hand, only have one grain.

Let's look at the definitions and terminologies that are important to grain and were discussed by George P Sutton:[1]

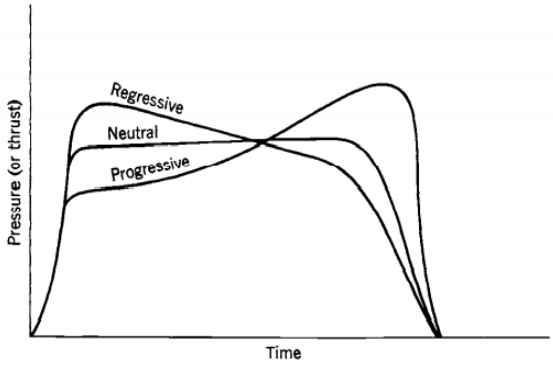

Fig. 2.1. Classification of grain according to their pressure (or thrust)- time characteristics.

Configuration: The shape or geometry of a grain's initial burning surfaces as they are supposed to function in a motor.

Cylindrical grain: The internal cross section of a grain remains constant along the axis despite of perforation form.

Neutral burning: Period during which the thrust, pressure, and burning surface area of the motor remain relatively

International Journal of Engineering Research & Technology (IJERT)
ISSN: 2278-0181
Vol. 10 Issue 06, June-2021

constant, usually within ±15 percent. Many grains burn in a neutral manner.

Progressive burning: Thrust, pressure, and burning surface area rises during the burn time.

Regressive burning: Thrust, heat, and burning surface area declines during the burn period.

Silver: Slivers are any unburned propellant that are left-out after combustion.

End-burning grains are typically used only in low-thrust, low-performance motors with long burn times. Their chamber diameter and dead weight are indeed high (intensive wall heating). Furthermore, during combustion, their centre of gravity changes. Nevertheless, with very fast-burning propellants, high-thrust, high-performance cigarette-burning motors may be considered. The combustion of a side-burning grain takes place on a straight cylinder shaped by the grain's lateral surfaces.

Since combustion occurs on almost all lateral surfaces, it is also known as unrestricted combustion (Table.2.1: A, B, C, D, E and F). Due to final grain fragmentation, the use of unregulated grains causes extreme wall heating and relatively high losses. The propellant itself is usually used to shield the walls in modern designs (Table.2.1: G, H, I, J, K, L, M, N and O). With this setup, wall heating can be kept to a minimum, if not entirely removed, resulting in very light chambers.

Side-burning grains are commonly referred to as cylindrical grains; although, such charges do not have to be cylindrical: for example, the axial grain load may be supported by a conical portion of the chamber, eliminating the need for the grid.

The grains that do not fit into any of the previous two categories fall into this group. It's distinguished by the fact that the burning area's generatrixes are no longer parallel straight lines. These types of grains are notoriously difficult to compute because they cannot be reduced to a two-dimensional problem.

Here we consider star-shape grain for our further discussion. The star shape optimization is usually a trade-off between sliver propellant mass, first-phase neutrality, and volumetric processing. The port area grows as the number of star points grows, with a subsequent reduction in the burning perimeter and the quantity of final sliver. For 3-to-5-star points, volumetric loading fractions in the range of 0.7 to 0.9 can be achieved. With increased volumetric loading, the sliver fraction increases dramatically [3].

The preliminary design of a solid propellant grain for a solid rocket motor must meet specifications expressed as a thrust versus time curve that takes into account available volume, temperature cycles, and other factors.[4]

By properly designing the propellant grain, the mechanical and thermal stresses in the grain can be reduced. Also, the physical properties of the propellant grain must thus be carefully evaluated in the choice of grain geometry.[5]

Many people have explained different theories and generated different equations to make the geometrical calculations for star-shape grain easy so that the parameters like thrust and chamber pressure versus time can be evaluated easily. The design calculations which were done on the star-shape grain are discussed in detail in following sections.

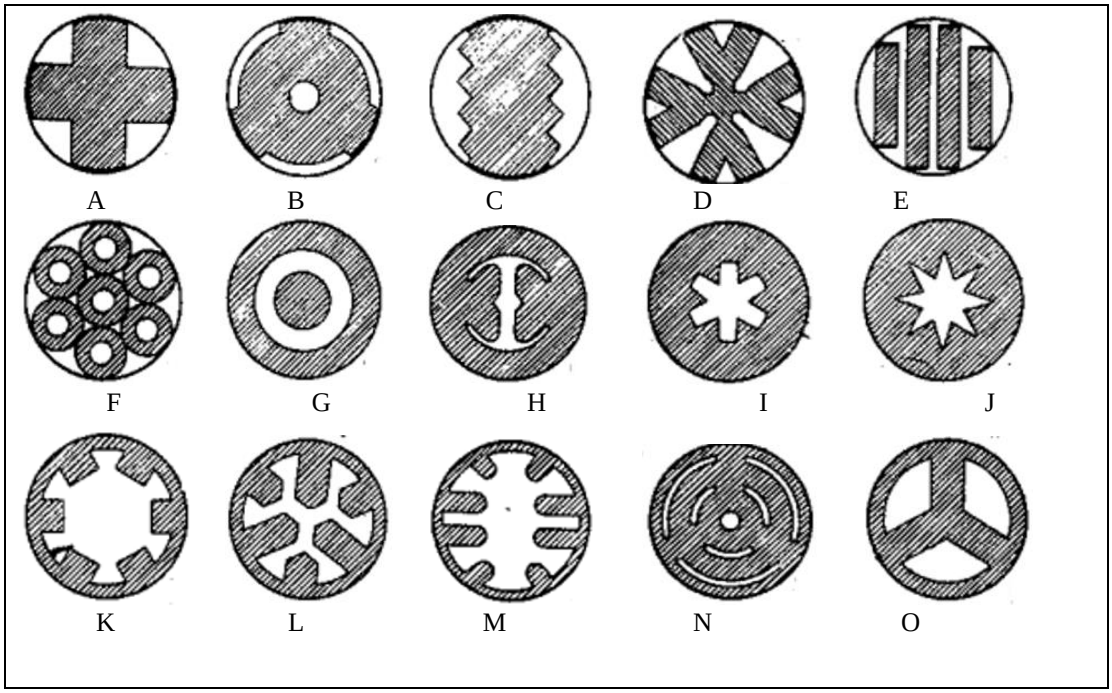

Table 2.1: Wide variety of grain cross-section.

International Journal of Engineering Research & Technology (IJERT)
ISSN: 2278-0181
Vol. 10 Issue 06, June-2021

3. METHODOLOGY

3.1 *Internal-burning stars* [2-6]

As mentioned in the previous chapter many people have explained different theories and generated different equations to make the geometrical calculations for star-shape grain easy so that the parameters like thrust and chamber pressure versus time can be evaluated easily. The design calculations which were done are studied in detail in this chapter. The design parameters of internal-burning star are shown in the form of figure 3.1.

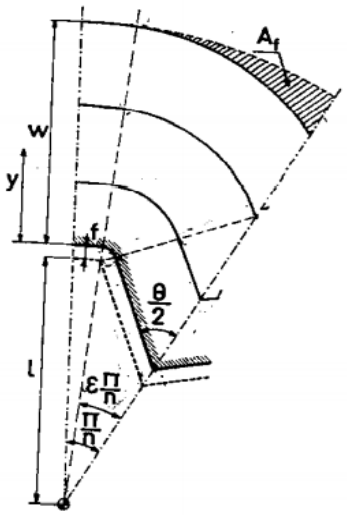

Fig. 3.1. Definition of the design parameters of an internal-burning star.

Number of star points – n
Web thickness – w
Maximum inner radius – $l + f$
Opening of star points - θ
Angular fraction - ε
Fillet radius – f

From the above fig. 3.1, several conclusions were illustrated.

a. In view of the progressive nature of combustion, the star with a fillet is identical to the same basic star (same n, l, ε and θ) without fillet which would have burnt over a distance f.
b. With the same initial perforation, the web can be increased without altering the beginning of the curve giving S as a function of y. It follows that the characteristic length to be selected to obtain dimensionless relationships is l.
c. The combustion is divided into two successive phases:
   - During first phase, the straight star points have not yet disappeared and, S can be progressive, neutral or regressive, depending upon the value of θ.
   - During second phase, the star points have disappeared and, shortly after transition, S becomes strongly progressive. Afterwards, when the burning front has reached the wall, relatively important tail-off takes place.

Table 3.1
Internal-burning star

A. *First phase*

$$for \quad \frac{y+f}{l} \le \frac{\sin\varepsilon\frac{\pi}{n}}{\cos\frac{\theta}{2}}$$

Burning perimeter:

$$\frac{S}{l} = 2n\left[\frac{\sin\varepsilon\frac{\pi}{n}}{\sin\frac{\theta}{2}} + \frac{y+f}{l}\left(\frac{\pi}{2} + \frac{\pi}{n} - \frac{\theta}{2} - cot\frac{\theta}{2}\right) + (1 - \varepsilon)\frac{\pi}{n}\right]$$

neutral burning for $\frac{\pi}{2} + \frac{\pi}{n} = \frac{\bar{\theta}}{2} + cot\frac{\bar{\theta}}{2}$

Initial port area:

$$\frac{A_p}{l^2} = n\sin\varepsilon\frac{\pi}{n}\left(\cos\varepsilon\frac{\pi}{n} - \sin\varepsilon\frac{\pi}{n}\cdot cot\frac{\theta}{2}\right) + (1-\varepsilon)\pi + 2n\frac{f}{l}\left[\frac{\sin\varepsilon\frac{\pi}{n}}{sin\frac{\theta}{2}} + (1-\varepsilon)\frac{\pi}{n} + 0.5\frac{f}{l}\left(\frac{\pi}{2} + \frac{\pi}{n} - \frac{\theta}{2} - cot\frac{\theta}{2}\right)\right]$$

B. *Second phase*

$$for \quad \frac{y+f}{l} \ge \frac{\sin\varepsilon\frac{\pi}{n}}{\cos\frac{\theta}{2}}$$

Burning perimeter:

$$\frac{S}{l} = 2n\left\{\frac{y+f}{l}\left[\frac{\pi}{n} + \sin^{-1}\left(\frac{l}{y+f}\cdot\sin\varepsilon\frac{\pi}{n}\right)\right] + (1-\varepsilon)\frac{\pi}{n}\right\}$$

Final losses:

$$\frac{A_f}{l^2} = \varepsilon\pi\left(1 + \frac{y+f}{l}\right)^2 - n\left\{\sin\varepsilon\frac{\pi}{n}\left[\sqrt{\left(\frac{y+f}{l}\right)^2 - sin^2\varepsilon\frac{\pi}{n}} + \cos\varepsilon\frac{\pi}{n}\right] + \left(\frac{y+f}{l}\right)^2\left[\varepsilon\frac{\pi}{n} + \sin^{-1}\left(\frac{l}{y+f}\cdot\sin\varepsilon\frac{\pi}{n}\right)\right]\right\}$$

and

$$\sigma_f = \frac{A_f/l^2}{\pi\left(1 + \frac{y+f}{l}\right)^2 A_{pi}/l^2}$$

Table 3.1 gives, the dimensionless form of burning perimeter S/l during the first and second phases, the port area A_p/l^2 during the first phase and the silver area A_f/l^2 during the second phase as functions of the reduced burnt distance (y + f)/ l and of the various design parameters.

International Journal of Engineering Research & Technology (IJERT)
ISSN: 2278-0181
Vol. 10 Issue 06, June-2021

Let us call $\bar{\theta}$ the value of θ for which neutrality is achieved during the first phase. The methodology used here is to generate a MATLAB code in order to find out burning perimeter, using burn perimeter to inner radius ratio S/l for star point n = 6 as per the conditions given. The MATLAB code is scripted in such a way that, for different combinations of *n, θ, f, l, ε* the graphs are plotted for burn perimeter (*S/l)* versus burnt distance (*y+f*)/*l*.

3.2 *Modelling and analysis*

As mentioned in the previous section. 3.1, the different combinations of *n, θ, f, l, ε* values are used to design the grain shape using computer aided designing software tool, CATIA- V5.

CATIA is the dominant current production solution across all engineering firms, like OEMs to independent small manufacturers, through their supply chains. CATIA's capabilities allow it to be used in a diverse range of companies, including aerospace, shipbuilding, plant design, and consumer goods, including design for items as diverse as jewellery and clothing.

Surface and form design, mechanical engineering, and equipment and systems engineering all benefit from CATIA's collaborative engineering capabilities. From subdivision, styling, and Class A surfaces to mechanical functional surfaces, CATIA offers a suite of surfacing, reverse engineering, and visualisation solutions to develop, alter, and validate complex innovative shapes.

From 3D sketches, sheet metal, composites, moulded, forged, or tooling components, to the concept of mechanical assemblies, CATIA enables the production of 3D parts. It includes methods for completing product specification, such as functional tolerances and kinematics.[7]

The star shape grain for n = 6, f = 0.5mm, ε = 0.74314, l = 15mm, w = 25mm, is designed using CATIA V5 software and the initial burning perimeter is measured using measuring tool for different θ values ranging between 65°-75°.[8]

Table 3.2

Star-shaped Propellant grain parameters

***n* = 6, *ε* = 0.74314, *l* = *15*mm, *f* = 0.5mm.**	
θ in degree	**Burning perimeter(*S*)** in mm
65	151.852
66	150.267
67	148.733
68	147.247
69	145.807
70	144.41
71	143.056
72	141.742
73	140.466
74	139.228
75	138.025

The star-shape propellant grain for n = 6, ε = 0.74314, l = *15*mm, f = 0.5mm, w = 25mm is designed in CATIA V5 designing tool. The values present in **Table 3.2** are the values obtained from CATIA V5 designing tool by measuring the burn perimeter at each star point angle from 65°-75°.

International Journal of Engineering Research & Technology (IJERT)
ISSN: 2278-0181
Vol. 10 Issue 06, June-2021

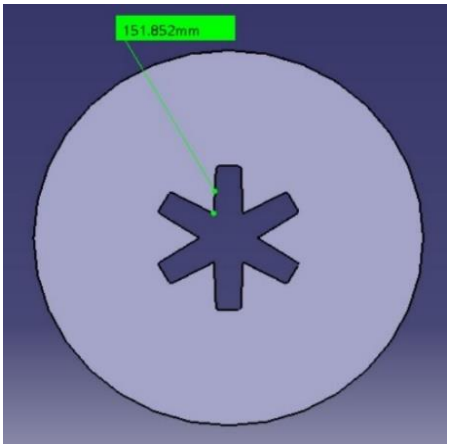

Fig.3.2.1 CATIA Model Star-grain θ=65°

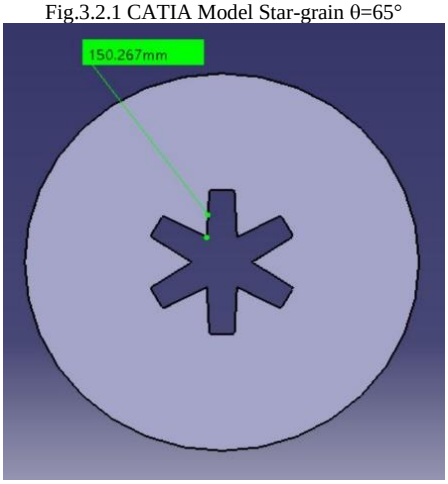

Fig.3.2.2 CATIA Model Star-grain θ=66°

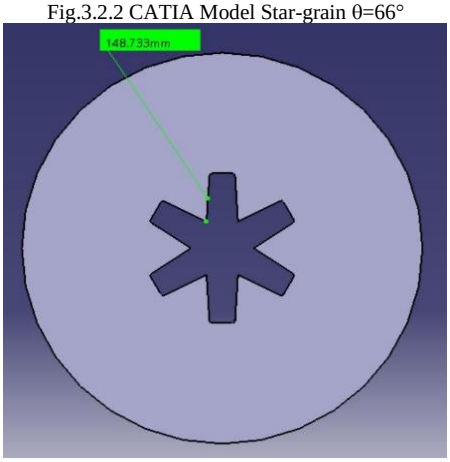

Fig.3.2.3 CATIA Model Star-grain θ=67°

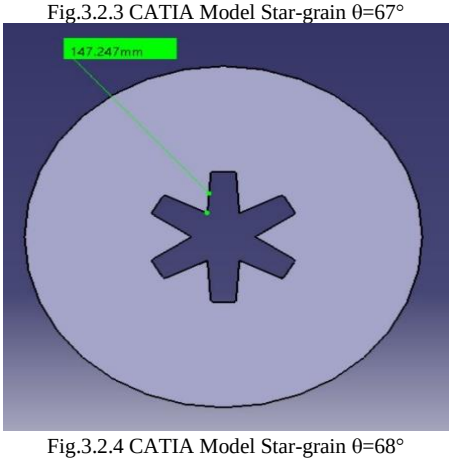

Fig.3.2.4 CATIA Model Star-grain θ=68°

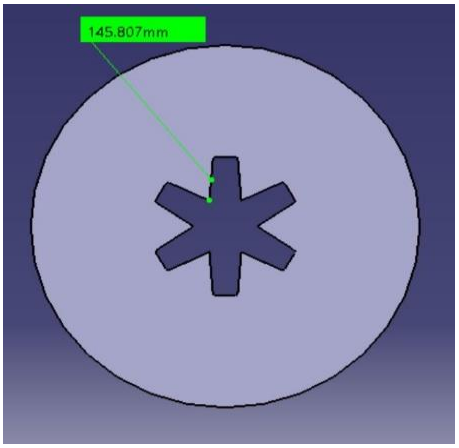

Fig.3.2.5 CATIA Model Star-grain θ=69°

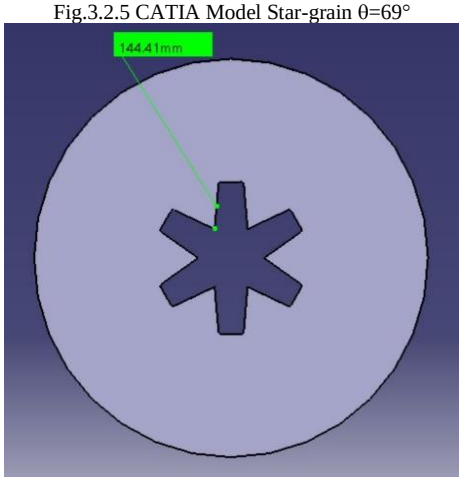

Fig.3.2.6 CATIA Model Star-grain θ=70°

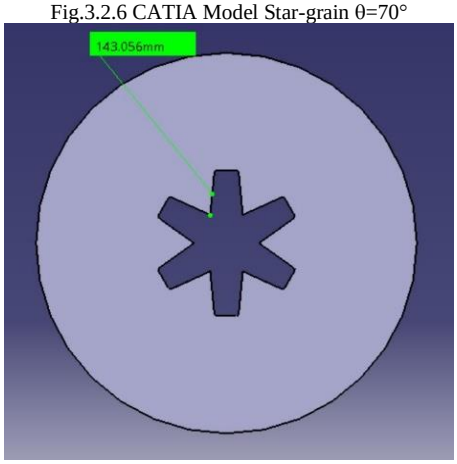

Fig.3.2.7 CATIA Model Star-grain θ=71°

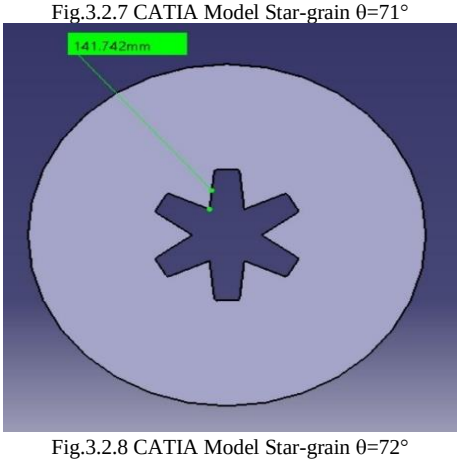

Fig.3.2.8 CATIA Model Star-grain θ=72°

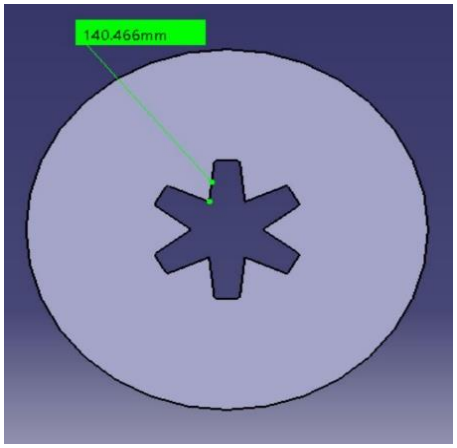

Fig.3.2.9 CATIA Model Star-grain θ=73°

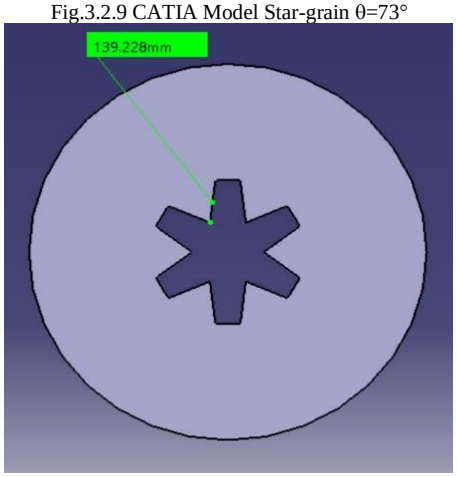

Fig.3.2.10 CATIA Model Star-grain θ=74°

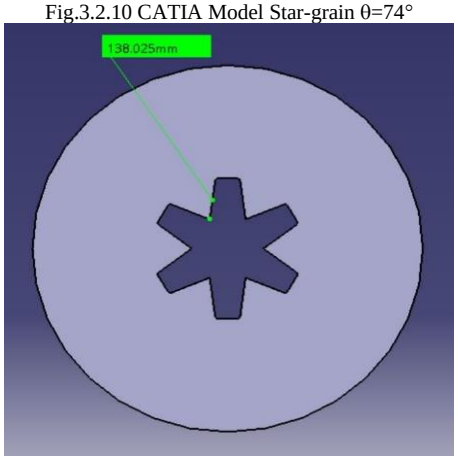

Fig.3.2.11 CATIA Model Star-grain θ=75°

International Journal of Engineering Research & Technology (IJERT)
ISSN: 2278-0181
Vol. 10 Issue 06, June-2021

3.2.1 AREA REGRESSION

Area regression for star-shaped propellant grain is analysed too.

For example, let n = 6, l = 15mm, θ = 67°, ε = 0.74314, w = 25mm, regression of propellant grain area due to combustion is visualized using CATIA V5 tool

.

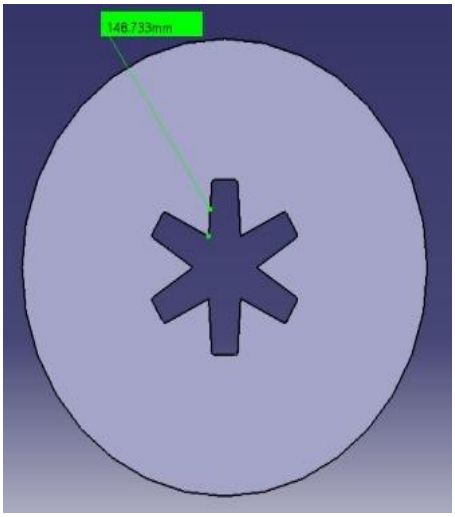

Figure 3.2.1(a) y = 0mm

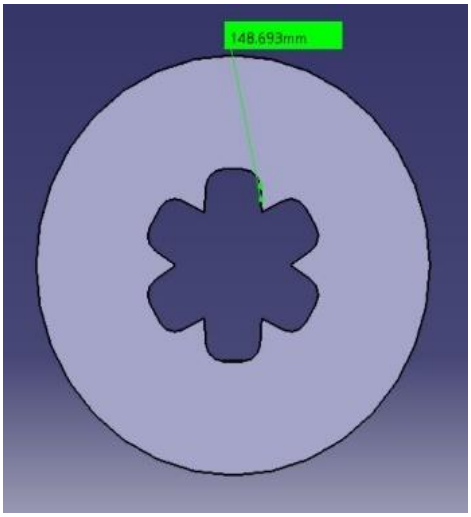

Figure 3.2.1(d) y = 3mm

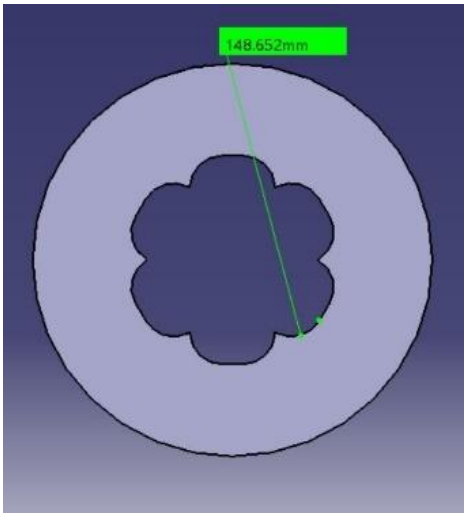

Figure 3.2.1(g) y = 6mm

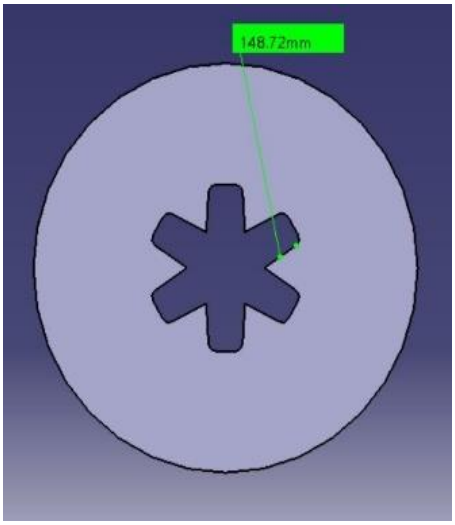

Figure 3.2.1(b) y = 1mm

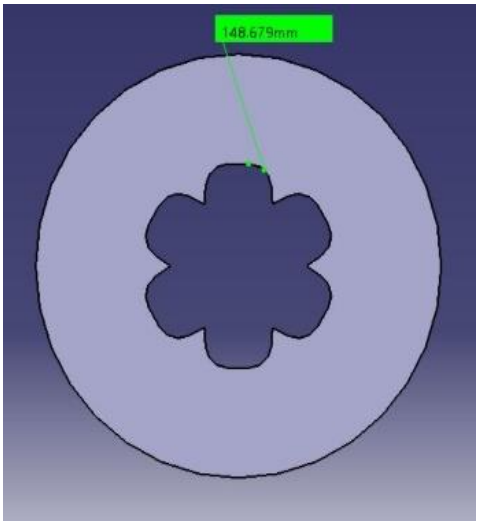

Figure 3.2.1(e) y = 4mm

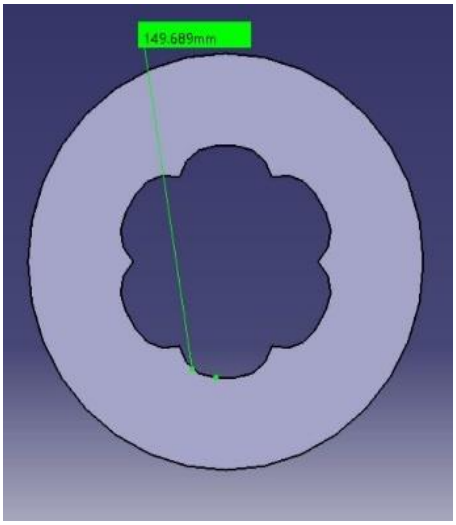

Figure 3.2.1(h) y = 7mm

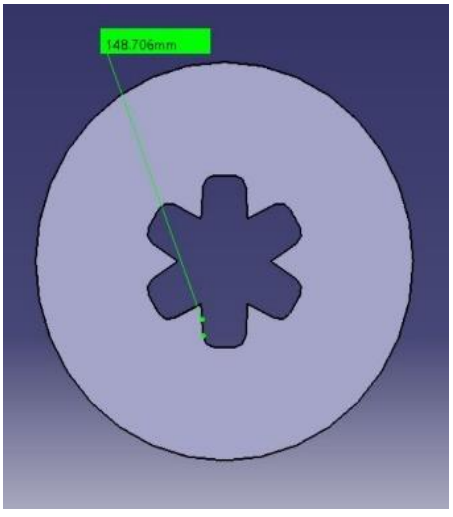

Figure 3.2.1(c) y = 2mm

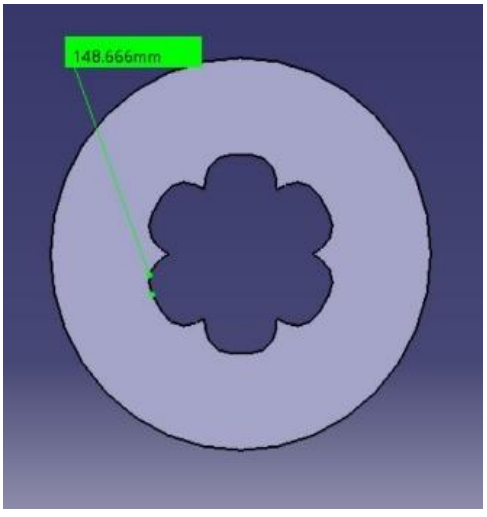

Figure 3.2.1(f) y = 5mm

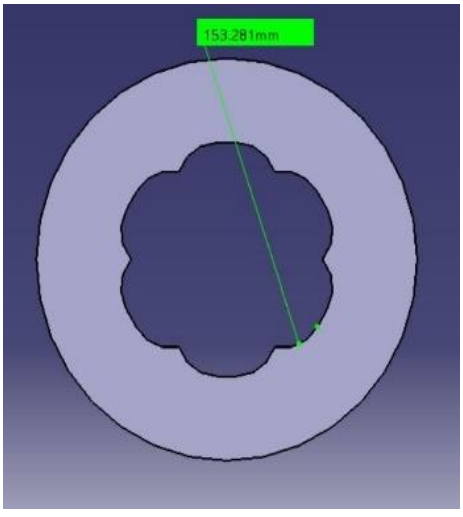

Figure 3.2.1(i) y = 8mm

International Journal of Engineering Research & Technology (IJERT)
ISSN: 2278-0181
Vol. 10 Issue 06, June-2021

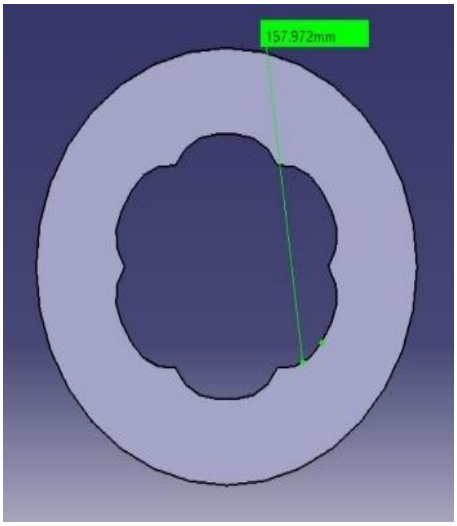

Figure 3.2.1(j) *y* = 9mm

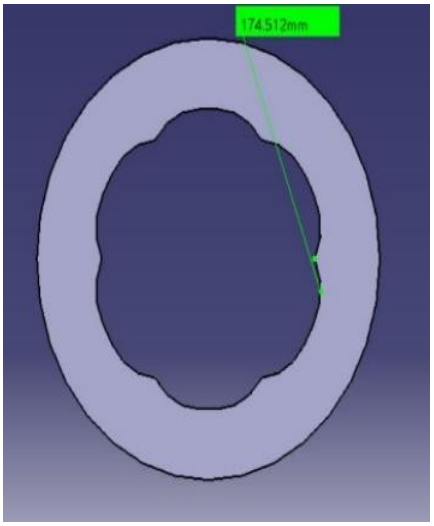

Figure 3.2.1(m) *y* = 12mm

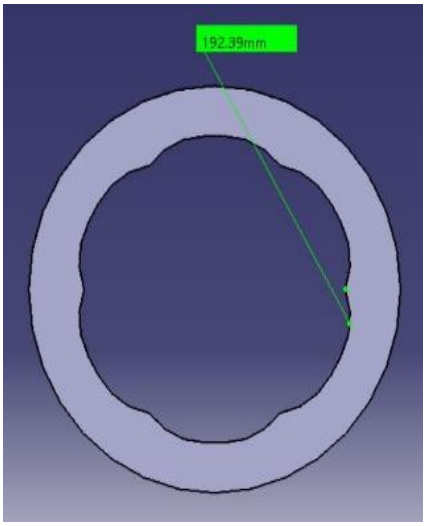

Figure 3.2.1(p) *y* = 15mm

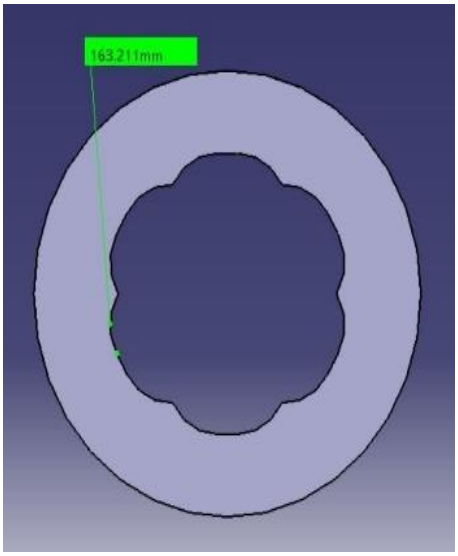

Figure 3.2.1(k) *y* = 10mm

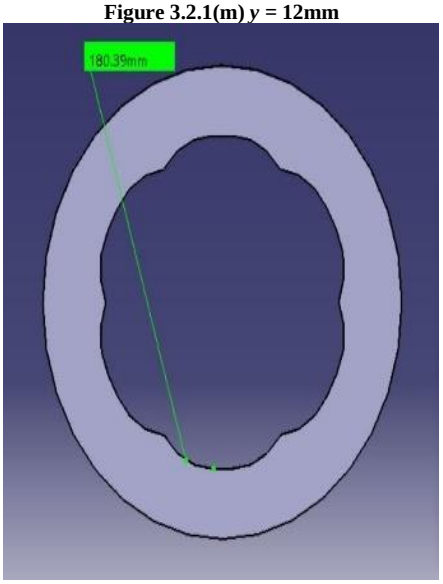

Figure 3.2.1(n) *y* = 13mm

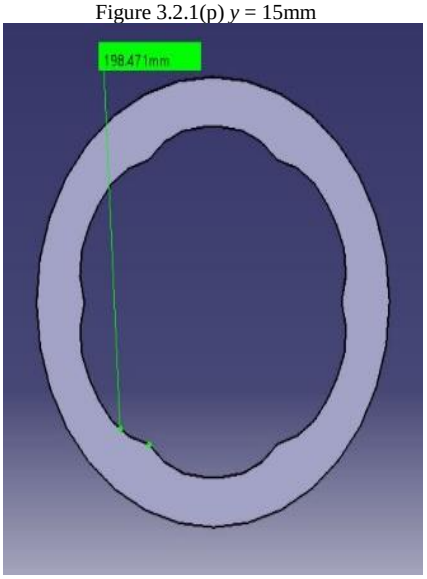

Figure 3.2.1(q) *y* = 16mm

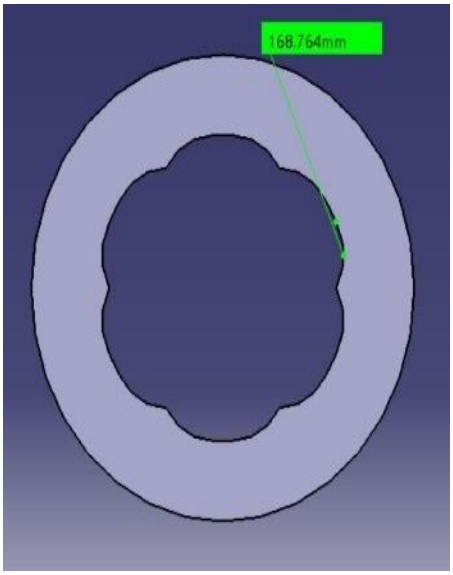

Figure 3.2.1(l) *y* = 11mm

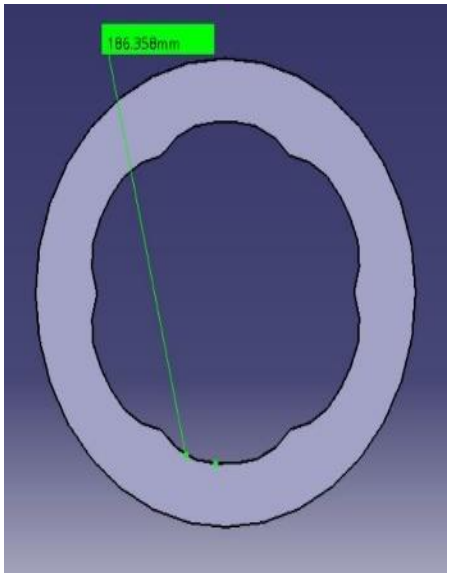

Figure 3.2.1(o) *y* = 14mm

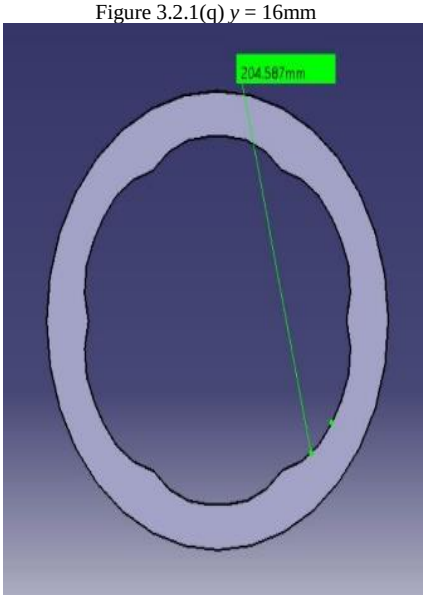

Figure 3.2.1(r) *y* = 17mm

International Journal of Engineering Research & Technology (IJERT)
ISSN: 2278-0181
Vol. 10 Issue 06, June-2021

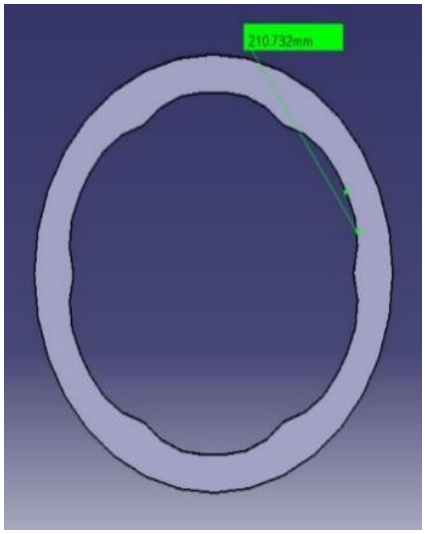

Figure 3.2.1(s) y = 18mm

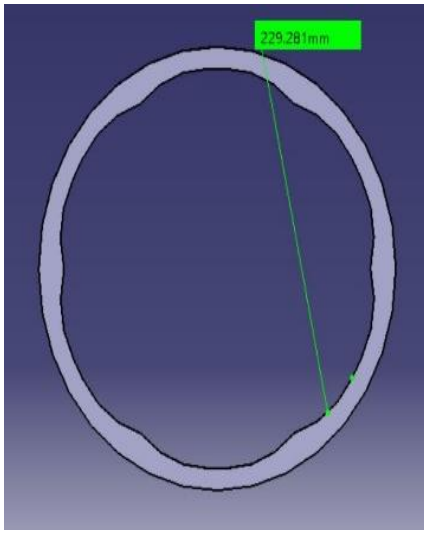

Figure 3.2.1(v) y = 21mm

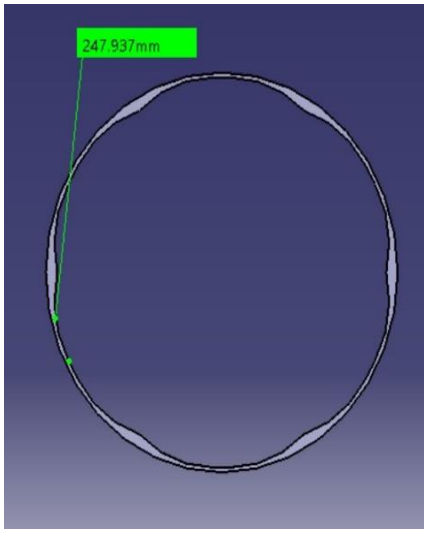

Figure 3.2.1(y) y = 24mm

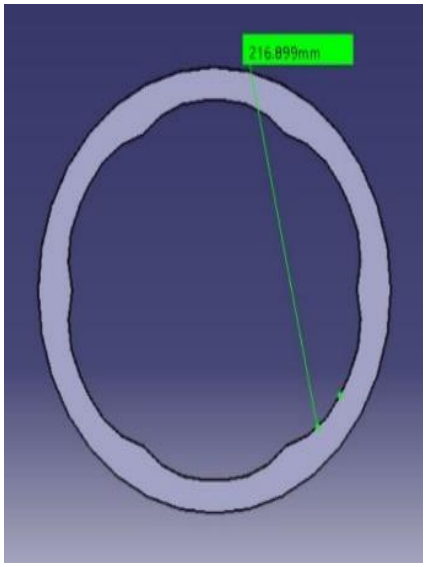

Figure 3.2.1(t) y = 19mm

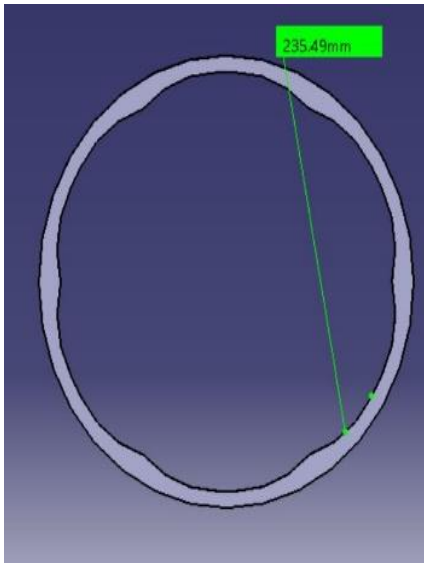

Figure 3.2.1(w) y = 22mm

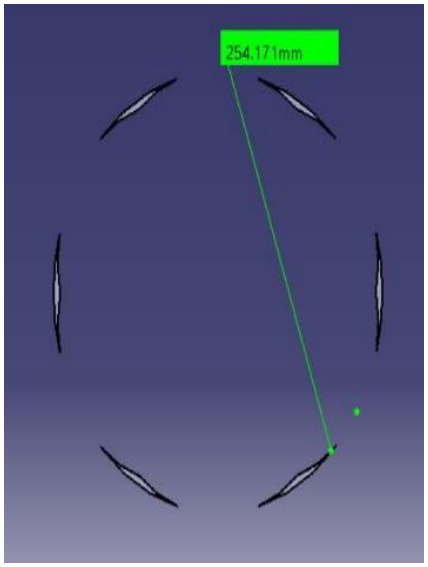

Figure 3.2.1(z) y = 25mm

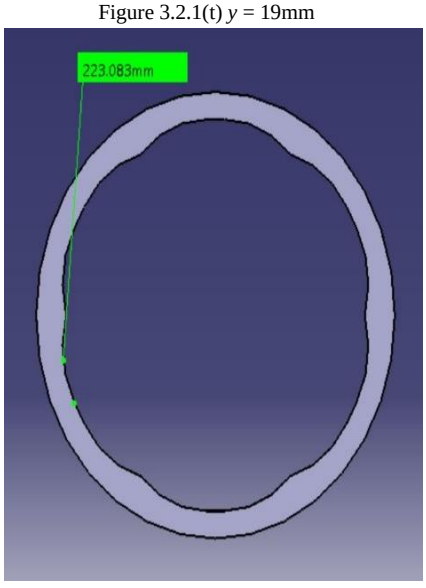

Figure 3.2.1(u) y = 20mm

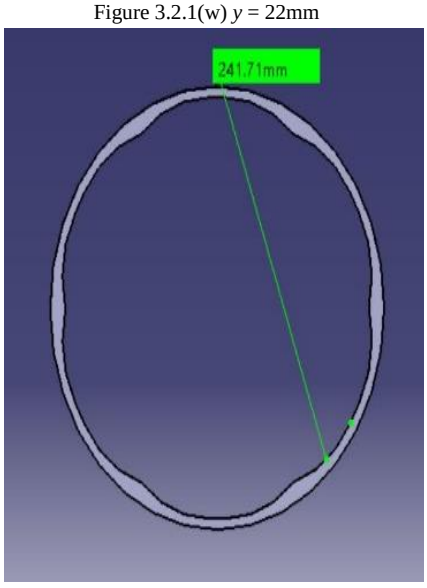

Figure 3.2.1(x) y = 23mm

International Journal of Engineering Research & Technology (IJERT)
ISSN: 2278-0181
Vol. 10 Issue 06, June-2021

MATLAB (*Matrix Laboratory*)

MATLAB is a fourth-generation scripting language and multi-paradigm numerical computing environment. Matrix transformations, plotting of various functionalities, implementation of algorithms, design of user interfaces, and syncing with programmes written in other languages, such as C, C++, Java, and Fortran, are all achievable with MATLAB, which has been developed by Math Works. While MATLAB is primarily designed for numerical computations, an optional toolbox that uses the MuPAD symbolic engine provides symbolic computing capabilities.

Simulink, a separate kit for dynamic and embedded systems, adds graphical multi-domain simulation and Model-Based Design.

Around one million of people used MATLAB across academia and industry in 2004. Users of MATLAB cover a wide range of engineering, science, and economics backgrounds. In both academic and industrial settings, MATLAB is commonly used.

In this project work, MATLAB code is programmed for a star shaped propellant grain such that the burn perimeter, port area, silver area is obtained for given set of parameters. From y =0 to 25 at 1mm increment, burn perimeter at each interval and corresponding θ value is evaluated and plots for each θ value are plotted. The plots obtained for different θ values are discussed in the next following section.

4. RESULTS AND DISCUSSION

The plots for non-dimensional burn perimeter (S/l) versus burnt distance $(y + f)/l$ are obtained from executing the above MATLAB code for n = 6, ε = 0.74314, l = 15mm, f = 0.5mm and θ ranging from 65°-75°.

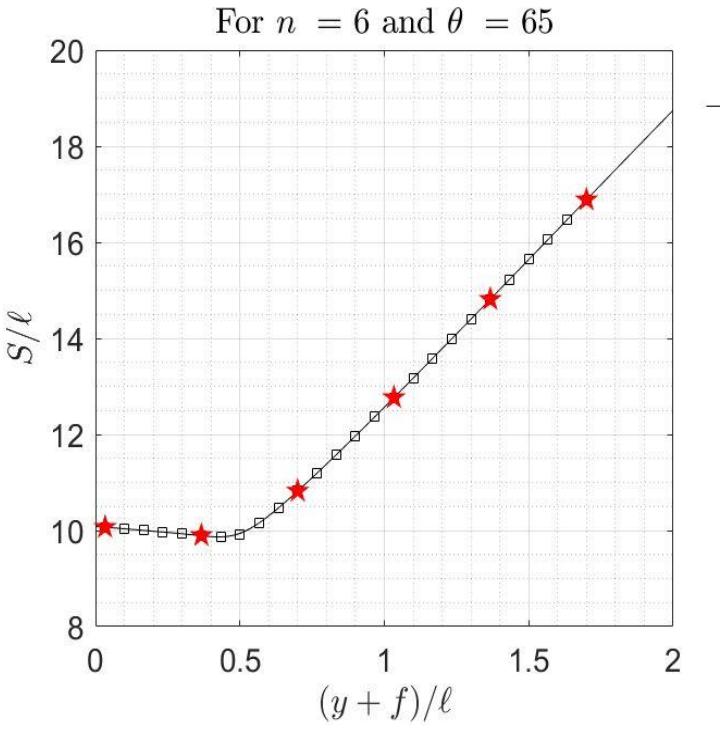

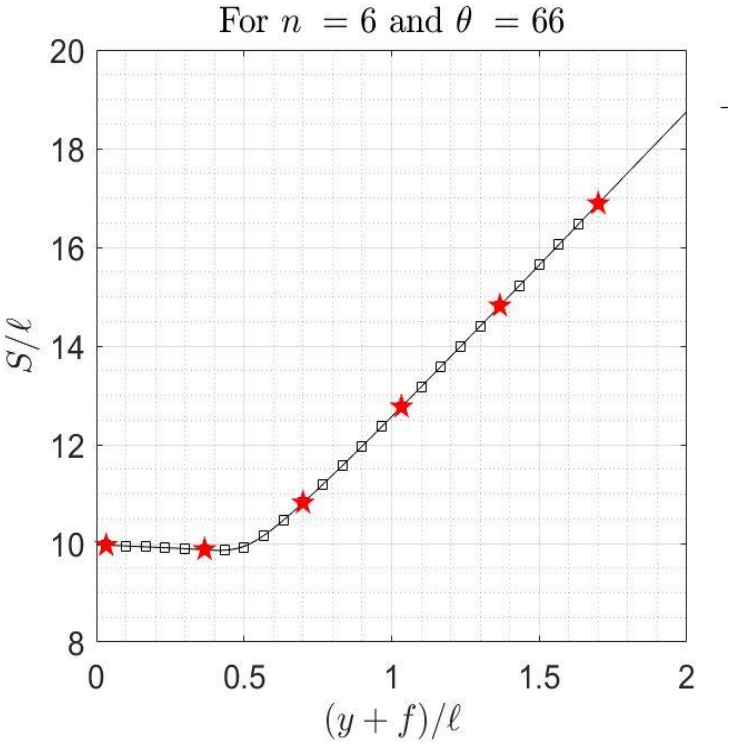

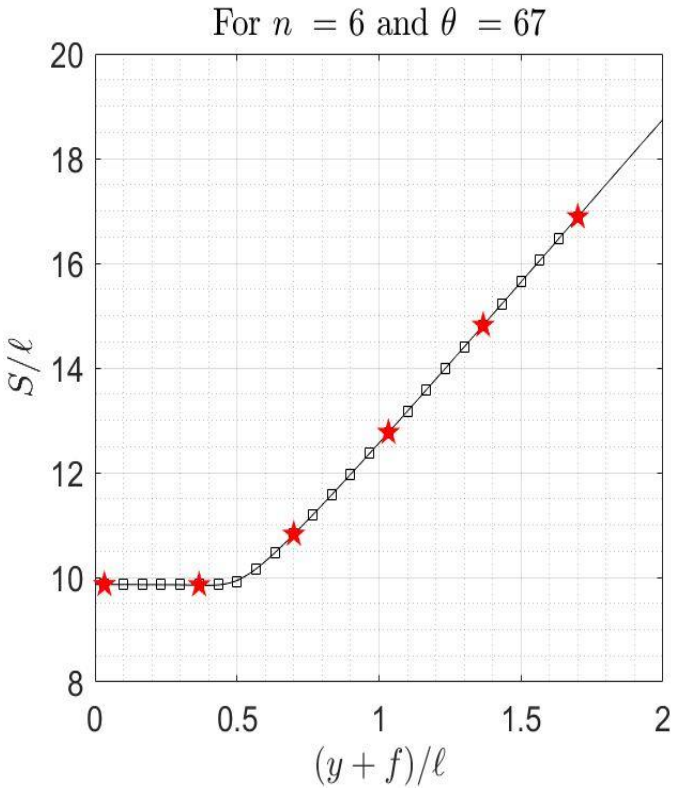

International Journal of Engineering Research & Technology (IJERT)
ISSN: 2278-0181
Vol. 10 Issue 06, June-2021

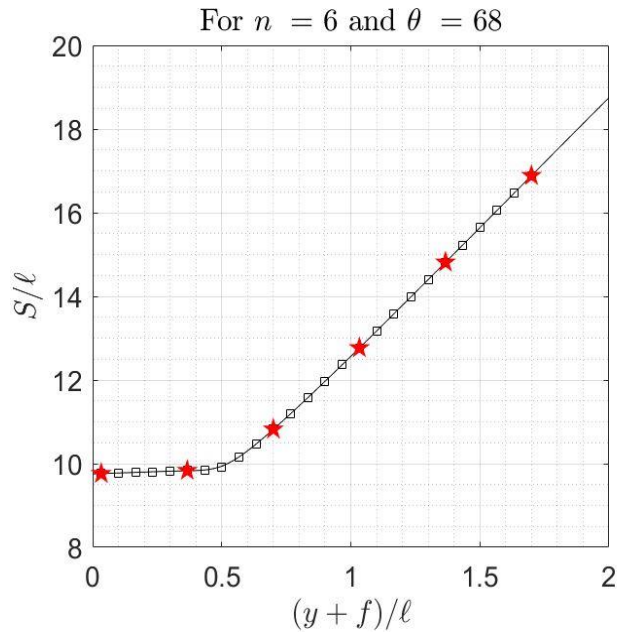

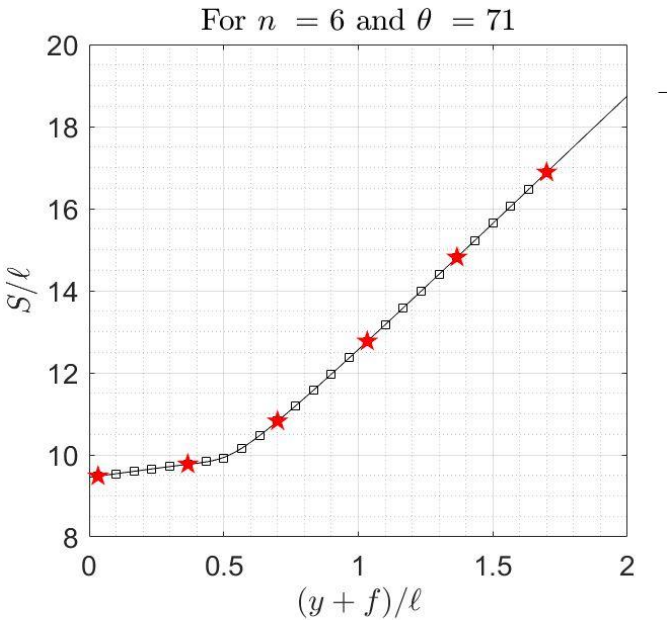

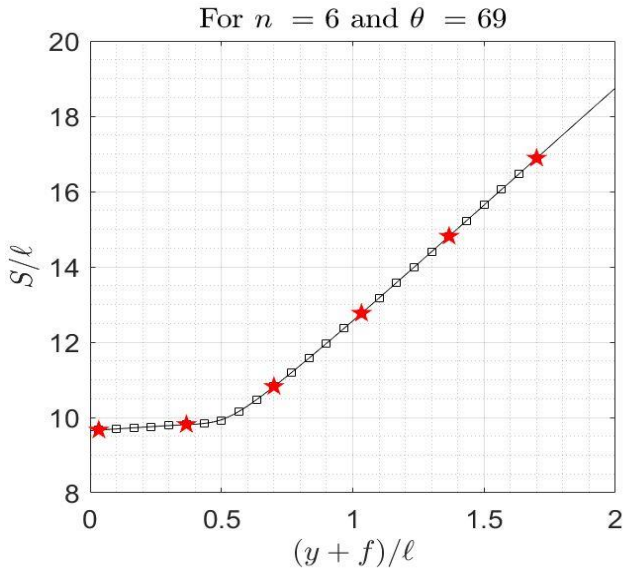

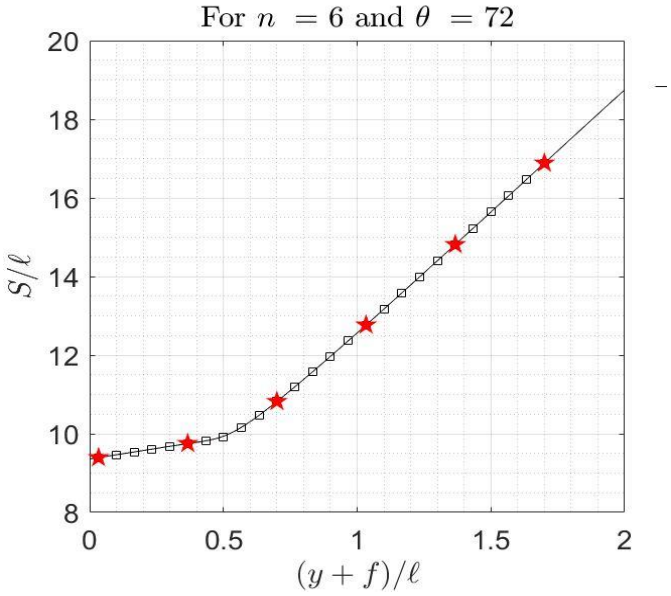

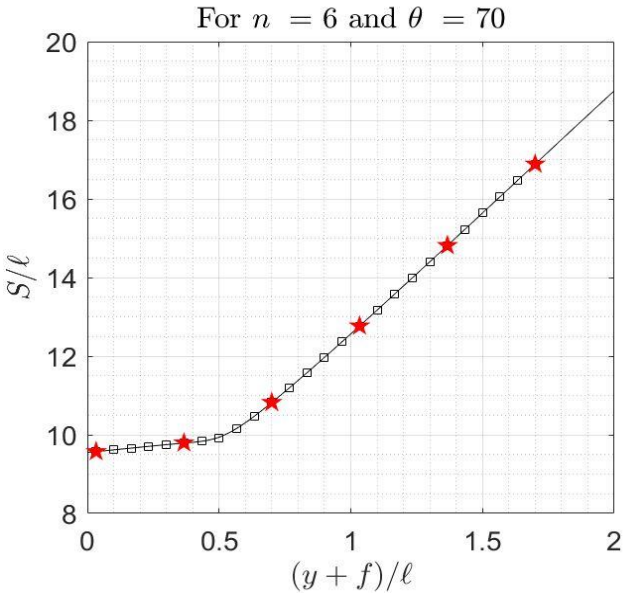

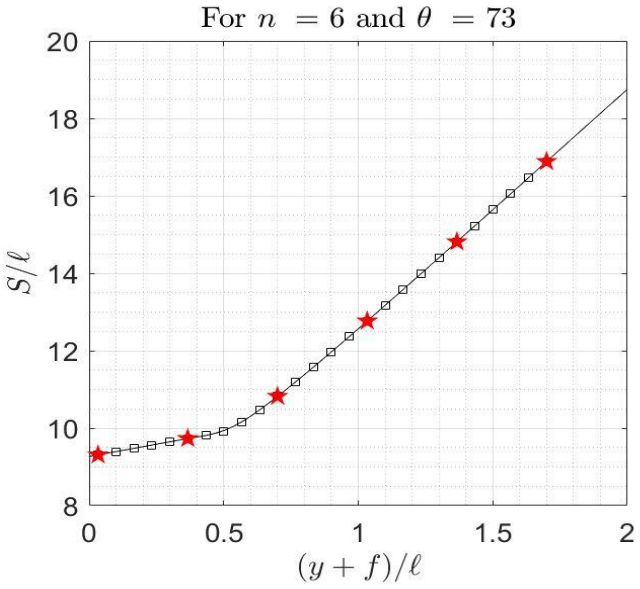

International Journal of Engineering Research & Technology (IJERT)
ISSN: 2278-0181
Vol. 10 Issue 06, June-2021

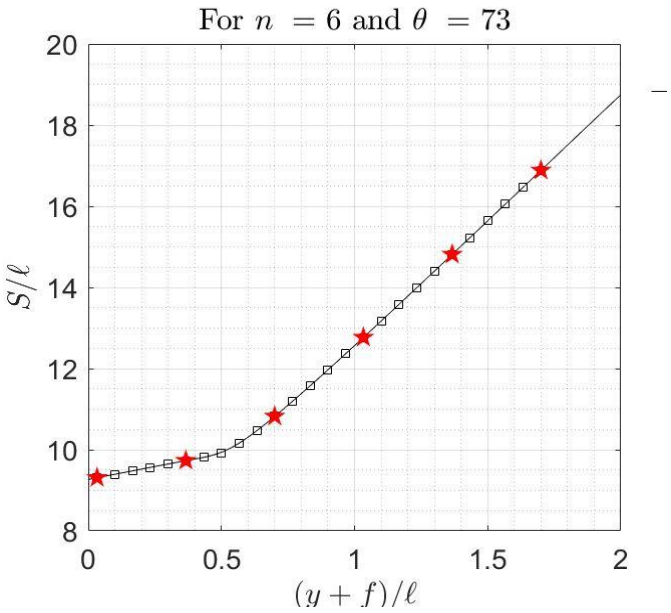

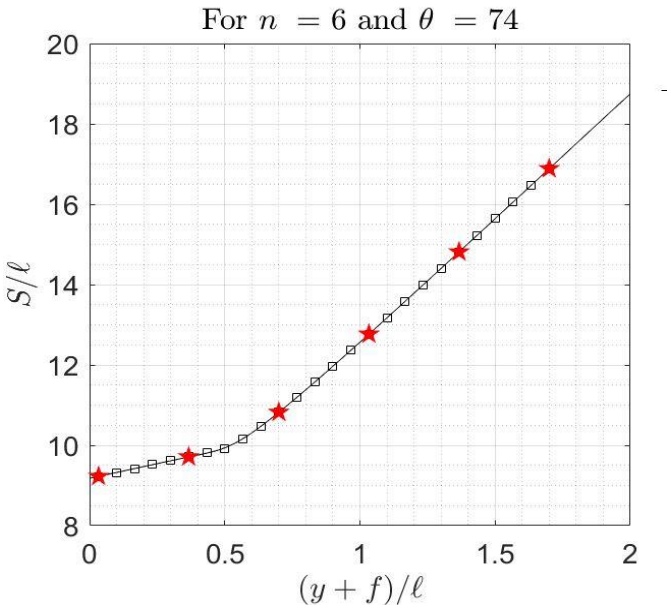

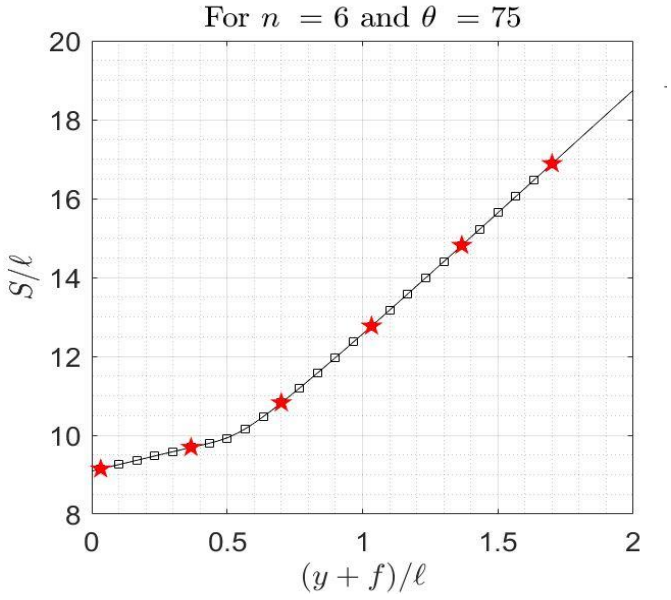

International Journal of Engineering Research & Technology (IJERT)
ISSN: 2278-0181
Vol. 10 Issue 06, June-2021

BURN PERIMETER VALUES OBTAINED FOR n = 6 AND θ = 65°-75°

θ=65°		*θ=66°*		*θ=67°*		*θ=68°*		*θ=69°*		*θ=70°*	
(S/l)	*S in mm*	*(S/l)*	*S in mm*	*(S/l)*	*S in mm*	*(S/l)*	*S in mm*	*(S/l)*	*S in mm*	*(S/l)*	*S in mm*
10.0695	151.0431	9.9638	149.457	9.8614	147.921	9.7622	146.433	9.6661	144.9908	9.5728	143.5925
10.0355	150.5328	9.9467	149.1998	9.8605	147.9075	9.7769	146.654	9.6958	145.4377	9.6171	144.2571
10.0015	150.0225	9.9295	148.9427	9.8596	147.894	9.7917	146.8751	9.7257	145.8847	9.6614	144.9216
9.967483	149.5122	9.9124	148.6856	9.8587	147.8805	9.8064	147.0962	9.756	146.3317	9.7058	145.5862
9.933465	149.002	9.8952	148.4284	9.8578	147.867	9.8212	147.3172	9.7852	146.7786	9.7501	146.2508
9.899447	148.4917	9.8781	148.1713	9.8569	147.8535	9.8359	147.5383	9.8150	147.2256	9.7944	146.9151
9.865429	147.9814	9.8609	147.9141	9.8559	147.84	9.8506	147.7594	9.8448	147.6726	9.8387	147.58
9.923613	148.8542	9.9236	148.8542	9.9236	148.8542	9.9236	148.8542	9.9236	148.8542	9.9236	148.8542
10.16208	152.4311	10.1621	152.4311	10.1620	152.4311	10.1621	152.4311	10.16207	152.4311	10.1621	152.4311
10.47430	157.1145	10.4743	157.1145	10.4743	157.1145	10.4743	157.1145	10.4743	157.1145	10.4743	157.1145
10.82324	162.3486	10.8232	162.3486	10.8232	162.3486	10.8232	162.3486	10.8232	162.3486	10.8232	162.3486
11.19319	167.8978	11.1932	167.8978	11.1932	167.8978	11.1932	167.8978	11.1932	167.8978	11.1932	167.8978
11.57625	173.6437	11.5762	173.6437	11.5762	173.6437	11.5763	173.6437	11.5763	173.6437	11.5763	173.6437
11.968	179.52	11.968	179.52	11.968	179.52	11.968	179.52	11.97	179.52	11.968	179.52
12.36578	185.4866	12.3658	185.4866	12.3658	185.4866	12.3658	185.4866	12.366	185.4866	12.3658	185.4866
12.76789	191.5183	12.7679	191.5183	12.7679	191.5183	12.7679	191.5183	12.7679	191.5183	12.768	191.5183
13.1732	197.598	13.1732	197.598	13.1732	197.598	13.1732	197.598	13.1732	197.598	13.1732	197.598
13.58093	203.714	13.5809	203.714	13.581	203.714	13.5809	203.714	13.5809	203.714	13.5809	203.714
13.99053	209.858	13.9905	209.858	13.9905	209.858	13.9905	209.858	13.9905	209.858	13.9905	209.858
14.4016	216.0242	14.4016	216.0242	14.4016	216.0242	14.4016	216.0242	14.4016	216.0242	14.4016	216.0242
14.8139	222.2078	14.8139	222.2078	14.8139	222.2078	14.8139	222.2078	14.8139	222.2078	14.8139	222.2078
15.2270	228.4057	15.2270	228.4057	15.2271	228.4057	15.2270	228.4057	15.2270	228.4057	15.2271	228.4057
15.6410	234.6151	15.6410	234.6151	15.6410	234.6151	15.6410	234.6151	15.6410	234.6151	15.6410	234.6151
16.0556	240.8342	16.0556	240.8342	16.0556	240.8342	16.0556	240.8342	16.0556	240.8342	16.0556	240.8342
16.4707	247.0611	16.4707	247.0611	16.4707	247.0611	16.4707	247.0611	16.4707	247.0611	16.4707	247.0611
16.8863	253.2948	16.8863	253.2948	16.8863	253.2948	16.8863	253.2948	16.8863	253.2948	16.8863	253.2948

International Journal of Engineering Research & Technology (IJERT)
ISSN: 2278-0181
Vol. 10 Issue 06, June-2021

θ=71°		θ=72°		θ=73°		θ=74°		θ=75°	
(*S*/*l*)	*S* in mm	(*S*/*l*)	*S* in mm	(*S*/*l*)	*S* in mm	(*S*/*l*)	*S* in mm	(*S*/*l*)	*S* in mm
9.4824	142.2363	9.3947	140.9205	9.31	139.6434	9.2269	138.4035	9.1466	137.1993
9.5407	143.1105	9.4665	141.9968	9.3943	140.9145	9.3242	139.8624	9.256	138.8392
9.599	143.9848	9.5382	143.0731	9.4790	142.1856	9.4214	141.3214	9.3653	140.4792
9.6573	144.8591	9.61	144.1495	9.5638	143.4568	9.5187	142.7803	9.4746	142.1195
9.7156	145.7333	9.6817	145.2258	9.6485	144.7279	9.616	144.2392	9.584	143.7595
9.7738	146.6076	9.7535	146.3021	9.7333	145.999	9.7132	145.6982	9.6933	145.3996
9.8321	147.4818	9.8252	147.3785	9.8180	147.2701	9.8105	147.1571	9.8026	147.0396
9.9236	148.8542	9.9236	148.8542	9.9236	148.8542	9.9236	148.8542	9.9236	148.8542
10.1621	152.4311	10.1621	152.4311	10.1621	152.4311	10.1621	152.4311	10.1621	152.4311
10.4743	157.1145	10.4743	157.1145	10.4743	157.1145	10.4743	157.1145	10.4743	157.1145
10.8232	162.3486	10.8232	162.3486	10.8232	162.3486	10.8232	162.3486	10.8232	162.3486
11.1932	167.8978	11.1932	167.8978	11.1932	167.8978	11.1932	167.8978	11.1932	167.8978
11.5763	173.6437	11.5762	173.6437	11.5762	173.6437	11.5763	173.6437	11.5763	173.6437
11.968	179.52	11.968	179.52	11.968	179.52	11.968	179.52	11.968	179.52
12.3658	185.4866	12.3658	185.4866	12.3658	185.4866	12.36578	185.4866	12.36578	185.4866
12.7679	191.5183	12.7679	191.5183	12.7679	191.5183	12.7679	191.5183	12.7679	191.5183
13.1732	197.598	13.1732	197.598	13.1732	197.598	13.1732	197.598	13.1732	197.598
13.5809	203.714	13.5809	203.714	13.5809	203.714	13.5809	203.714	13.5809	203.714
13.991	209.858	13.9905	209.858	13.9905	209.858	13.9905	209.858	13.9905	209.858
14.4016	216.0242	14.4016	216.0242	14.4016	216.0242	14.4016	216.0242	14.4016	216.0242
14.8139	222.2078	14.8139	222.2078	14.8139	222.2078	14.8139	222.2078	14.8139	222.2078
15.2271	228.4057	15.2271	228.4057	15.2270	228.4057	15.2271	228.4057	15.2271	228.4057
15.6410	234.6151	15.6410	234.6151	15.6410	234.6151	15.6410	234.6151	15.6410	234.6151
16.0556	240.8342	16.0556	240.8342	16.0556	240.8342	16.0556	240.8342	16.0556	240.8342
16.4707	247.0611	16.4707	247.0611	16.4707	247.0611	16.4707	247.0611	16.4707	247.0611
16.8863	253.2948	16.8863	253.2948	16.8863	253.2948	16.8863	253.2948	16.8863	253.2948

5. CONCLUSION

The burn perimeter obtained from the MATLAB code are compared with the burn perimeter measured in CATIA V5 software using measuring tool. It is observed that:

- The values for burn perimeter obtained through MATLAB is exactly same when measured in CATIA designing tool.
- The results acquired concludes that the particular MATLAB code is correct and can be used to calculate the burn perimeter, port area, silver area, not only for n=6 but also for different star point numbers 7, 8, 9, 10, 11, 12 and with different combinations of θ, ε, f, l, w as inputs. But from the observations made, for n = 6, f = 0, ε = 1, the star point angle θ is limited to 30°. Similarly, it is impossible for n = 5, f =0 and $\theta = \bar{\theta}$ to have $\varepsilon > 0.875$.
- From the plots obtained, for example n = 6:
  - It is seen that for θ = 65° and 66°, during first phase the burn perimeter is regressive and during the second phase burn perimeter is strongly progressive.
  - For θ = 67°, during first phase the burn perimeter is neutral whereas during second phase i.e., from **Figure 3.2.1(h) y = 7mm** the burn perimeter is strongly progressive.
  - For θ = 68°, 69°, 70°, 71°, 72°, 73°, 74° and 75°, during first phase the burn perimeter is progressive and after disappearing of star points i.e., during second phase the burn perimeter is strongly progressive.
- In addition to this, one more observation that is made by using MATLAB code is that, n and θ values play role on the burn perimeter but the epsilon (ε) and fillet radius f plays a major role and are responsible for transition between phase I and II irrespective of variation in n and θ values.

6. FURTHER WORK [9]

Enrico Cavallini has developed an analysis/simulation capability of SRM internal ballistic for the entire combustion time, with simplified physical models. The burn perimeter obtained through MATLAB code for the design parameters as per propulsion requirements are used to calculate the pressure and thrust versus time using incremental analysis.

$$\frac{P_c A_t}{C^*} = \rho_p A_b \dot{r}$$

$$T = \dot{m}_e V_e - (P_e - P_a) A_e$$

In order to solve for thrust and chamber pressure, the throat area, burn surface area, mass flow rate discharged through nozzle, are calculated by solving for quasi 1D unsteady flow field conservation, momentum and energy equations at each Δx increment.

$$\frac{\partial(\rho A_p)}{\partial t} + \frac{\partial(\rho u A_p)}{\partial x} = r_b P_b \rho_P + \frac{\dot{m}_s A_p}{V} + \frac{\dot{m}_{ig} A_p}{V}$$

$$\frac{\partial(\rho u A_p)}{\partial t} + \frac{\partial[(\rho u^2 + p) A_p]}{\partial x} - P\frac{\partial A_p}{\partial x} = \frac{\dot{m}_{ig} A_p \bar{v}_{inj}}{V} + \frac{1}{2}\rho u^2 c_F P_w$$

$$\frac{\partial(\rho E A_p)}{\partial t} + \frac{\partial[(\rho E + p) u A_p]}{\partial x} = r_b P_b \rho_P h_f + \frac{\dot{m}_{ig} A_p H_{ig}}{V} + \frac{\dot{m}_s A_p H_s}{V}$$

International Journal of Engineering Research & Technology (IJERT)
ISSN: 2278-0181
Vol. 10 Issue 06, June-2021

7. APPENDIX

MATLAB PROGRAMME

```
clc
clear
close all
disp('Internal Burning Star with thby2 in Degrees');
disp('-------------------------------------------------');
disp('Inut Parameters are ');
disp('-------------------------------------------------');
%%
l   = 15;
w   = 25;
f   = 0.5;
eps = 0.74314;
n   = 6;

thby2 = deg2rad(68/2);
yn    = 26;
y     = transpose(linspace(0,w,yn));
disp(['Length          = ',num2str(l),' mm']);
disp(['Width           = ',num2str(w),' mm']);
disp(['Fillet          = ',num2str(f),' mm']);
disp(['Epsilon         = ',num2str(eps)]);
disp(['Number of stars  = ',num2str(n)]);
disp(['Theta           = ',num2str(rad2deg(thby2*2)),' Â°']);
disp('-------------------------------------------------');
%%
disp('-------------------------------------------------');
disp('Calculating the combustions parameters for y ');
disp('-------------------------------------------------');
for i = 1:numel(y)
   LHS(i,:) = (y(i)+f)./(l);
   for j = 1:numel(thby2)
      const(j,1) = eps*(pi/n);
      RHS(j)   = sin(eps*(pi/n))/cos(thby2(j));
      if LHS(i,:) <= RHS(j)
         disp('Combustion in Phase I')
         BP(i,:) = ((2*n)*((sin(eps*(pi/n))/sin(thby2(j)))+...
            (LHS(i,:)*((pi/2)+(pi/n)-(thby2(j))-...
            cot(thby2(j)))+((1-eps)*(pi/n)))));
         disp(['BP = ',num2str(BP(i,:)*l),' mm at y =
',num2str(y(i)), ' mm']);
         IPA(:,j)  = (abs(n*sin(const(j)))*(cos(const(j))-...
            (sin(const(j))*cot(thby2(j)))))+((1-eps).*pi)+...
            ((2*n*(f/l))*((sin(eps*(pi/n))/sin(thby2(j)))+...
            ((1-eps)*(pi/n))+((0.5*(f/l))*((pi/2)+(pi/n)-
(thby2(j))-...
            cot(thby2(j))))));
      elseif LHS(i,:) >= RHS(j)
         disp('Combustion in Phase II')
         BP(i,:) =
(2*n)*((LHS(i,:)*((pi/n)+asin((1/LHS(i,:))*(sin(const(j)))))
)+...
            ((1-eps)*(pi/n)));
         disp(['BP = ',num2str(BP(i,:)*l),' mm at y =
',num2str(y(i)), ' mm']);
         FL(:,j) = (eps*pi*((1+LHS(i,:))^2))-...
            n*((sin(const(j))*((sqrt(LHS(i,:)^2-
(sin(const(j))^2)))+...
            cos(const(j))))+
((LHS(i,:)^2)*(const(j)+asin((1/RHS(j))*(sin(const(j)))))));
         sigf(i,:) = FL(1,j)/((pi*((1+LHS(i,:))^2))-
((IPA(1,j))/(l^2)));
      end
   end
end
disp('-------------------------------------------------');
disp('              End of calculation!              ');
disp('-------------------------------------------------');
% return
%% Plotting results
disp('-------------------------------------------------');
disp('           Plotting the Burn Perimeter!        ');
disp('-------------------------------------------------');
ft = fittype( 'smoothingspline' );
opts = fitoptions( 'Method', 'SmoothingSpline' );
opts.SmoothingParam = 0.0233503103188522;
[ftr,gof] = fit(LHS,BP,ft);
% return
ind_trans = find(LHS(:,1)>RHS);
figure('color','w');
set(gca,'fontsize',14);
hold on
plot(LHS, BP,'sk');
plot(ftr,'-k');
plot(LHS(1),
BP(1),'pr','MarkerFaceColor','r','MarkerSize',10);
plot(LHS(6),
BP(6),'pr','MarkerFaceColor','r','MarkerSize',10);
plot(LHS(11),
BP(11),'pr','MarkerFaceColor','r','MarkerSize',10);
plot(LHS(16),
BP(16),'pr','MarkerFaceColor','r','MarkerSize',10);
plot(LHS(21),
BP(21),'pr','MarkerFaceColor','r','MarkerSize',10);
plot(LHS(26),
BP(26),'pr','MarkerFaceColor','r','MarkerSize',10);
xlabel('$(y+f)/\ell$','Interpreter','Latex')
ylabel('$S/\ell$','Interpreter','Latex');
title(['For $n\ =\ $',num2str(n),' and $\theta\ =\ $',...
   num2str(rad2deg(thby2*2))],'Interpreter','Latex')
lgn = legend('Data','Fit');
set(lgn,'Interpreter','Latex','Location','BestOutside','EdgeCo
lor','w');
grid on
grid minor
box on
```

REFERENCES

[1] GEORGE P. SUTTON., "Rocket Propulsion Elements," California: John Wiley & Sons, 2001, 7th edition, Ch 1, pp. 1-6.
[2] M. Barrere., Jaumotte. A., B. Fraeijs De Veubeke., Vandenkerckhove. J., "Rocket Propulsion," Paris: Elsevier, 1960, Ch 1: pp 1-6, Ch 4: pp 190-205, Ch 6: 291-308.
[3] Makled. A., El -Senbawi. M. A., Abdalla. H. M., "Evaluation of Design Parameters of The Solid Propellant Star Grain Configuration," ASAT Conference, 10th volume, pp. 243-245, 13-15 May 2003.
[4] G. Uhrig., B. Ducourneau and P. Liesa., "Computer Aided Preliminary Design of Propellant Grains for Solid Rocket Motors,"

International Journal of Engineering Research & Technology (IJERT)
ISSN: 2278-0181
Vol. 10 Issue 06, June-2021

AIAA/SAE/ASME/ASEE 23rd Joint Propulsion Conference, AIAA-87-1734, pp. 1-3, June 29- July 2 1987.

[5] JEAN A. VANDENKERCKHOVE., "Recent Advances in Solid Propellant Grain Design," ARS Journal, DOI: 10.2514/8.4810, pp. 1-4, 1959.

[6] MAX W. STONE., "A Practical Mathematical Approach to Grain Design," ARS Semi-Annual Meeting, DOI: 10.2514/8.7285, pp. 236-239, June 10-13 1957.

[7] Patan Stalin., Y.N.V.Santosh Kumar and SK.Nazumuddin., "Design and Geometrical Analysis of Propellant Grain Configurations of a Solid Rocket Motor," International Journal of Engineering Development and Research, ISSN: 2321-9939, Volume 2, Issue 4, pp. 3418-3419, 2014.

[8] Anwer Hashish., Mahmoud Yehia Mohamed., Hamed M. Abdalla and Mohamed Allam Al-Sanabawy., "Design of Solid Propellant Grain for Predefined Performance Criteria," AIAA SciTech Forum, m 7-11 January 2019, DOI: 10.2514/6.2019-2014, pp. 6-10, 7-11 January 2019.

[9] Enrico Cavallini., Maurizio DI Giacinto., " Modeling And Numerical Simulation Of Solid Rocket Motors Internal Ballistics," [Ph.D. thesis], Sapienza Universita DI Rome, Rome, Italy, 2010.